NASA
Technical
Paper
3018

August 1990

An Approximate Method for Calculating Three-Dimensional Inviscid Hypersonic Flow Fields

Christopher J. Riley
and Fred R. DeJarnette

NASA

NASA Technical Paper 3018

1990

An Approximate Method for Calculating Three-Dimensional Inviscid Hypersonic Flow Fields

Christopher J. Riley
Langley Research Center
Hampton, Virginia

Fred R. DeJarnette
North Carolina State University
Raleigh, North Carolina

National Aeronautics and Space Administration
Office of Management
Scientific and Technical Information Division

Abstract

An approximate solution technique has been developed for three-dimensional, inviscid, hypersonic flows. The method uses Maslen's explicit pressure equation and the assumption of approximate stream surfaces in the shock layer. This approximation represents a simplification of Maslen's asymmetric method. The present method presents a tractable procedure for computing the inviscid flow over three-dimensional surfaces at angle of attack. The solution procedure involves iteratively changing the shock shape in the subsonic-transonic region until the correct body shape is obtained. Beyond this region, the shock surface is determined by using a marching procedure.

Results are presented herein for a spherically blunted cone, a paraboloid, and an elliptical cone at angle of attack. The calculated surface pressures are compared with experimental data and finite-difference solutions of the Euler equations. Shock shapes and profiles of pressure are also examined. Comparisons of the results of the present method with experimental data and detailed predictions are very good. Since the present method provides a very rapid computational procedure, it can be used for parametric or preliminary design applications. A useful application would be to incorporate a heating procedure for aerothermal studies.

Introduction

An approximate solution of the three-dimensional (3-D) inviscid flow-field equations for hypersonic speeds is an important design tool, especially for the prediction of surface heating rates on reentry vehicles. Coupled inviscid-viscous calculations have been demonstrated to adequately predict the heating over a wide range of aerothermal environments. (See refs. 1 to 3.) The 3-D inviscid solutions used by these engineering aeroheating methods differ in complexity from simple modified Newtonian theory (ref. 1) to more exact finite-difference solutions of the 3-D Euler equations (refs. 3 and 4). Modified Newtonian theory is simple to use, but its accuracy is limited. Finite-difference solutions of the inviscid equations (refs. 4 to 7) may be too computer-intensive for a preliminary design study. A rapid but accurate 3-D inviscid analysis would significantly enhance current engineering aerothermal capabilities.

Surface heating rates on reentry vehicles may also be obtained by numerically solving the full 3-D Navier-Stokes equations. (See ref. 8.) Solutions to the various subsets of the Navier-Stokes equations, including the parabolized Navier-Stokes (ref. 9) and viscous shock-layer (refs. 10 to 12) equations, have also been obtained for 3-D flows. Although these methods yield good results, they require excessive computer storage and CPU (central processing unit) time to be practical for a preliminary-design environment in which a range of geometries and flow parameters are to be studied. An approximate 3-D inviscid method coupled with an engineering aeroheating prediction method can easily be run on a computer workstation and complements the more accurate CFD (computational fluid dynamics) methods in the design of reentry vehicles.

Maslen (ref. 13) developed an approximate inviscid flow-field method for axisymmetric bodies in the early 1960's. From simplifications made for hypersonic speeds, Maslen obtained an explicit expression for the first-order pressure along lines normal to the shock wave. Since the body shape is determined from a given shock shape, this method is referred to as an inverse technique. Solving for a specified body shape can be accomplished indirectly by iteration of the shock shape. (See refs. 14 and 15.) This technique gives reasonable results, but the first-order pressure equation is inaccurate on the conical afterbody of a spherically blunted cone.

Maslen subsequently outlined a method for three-dimensional inviscid flow (ref. 16), and improved the explicit pressure equation by deriving a second-order approximation of the momentum equation normal to the shock. Although more accurate, the 3-D method is complicated and unwieldy. In fact, only preliminary results were presented for blunt-body flows. (See refs. 17 and 18.)

The present analysis simplifies the asymmetric problem by using two stream functions that approximate the actual stream surfaces in the shock layer and a reduced form of the Maslen second-order pressure equation. Thus, the present method, while applicable to three-dimensional flows, retains the utility and accuracy of Maslen's axisymmetric technique. Comparisons of the present results in terms of pressure profiles, surface distributions, and corresponding shock shapes are presented with Euler predictions and experimental data for spherically blunted cones, ellipsoids, and paraboloids at angle of attack.

Symbols

B, b, c, d	conic section parameters (eqs. (19) and (20))
$\mathbf{e}_x, \mathbf{e}_r, \mathbf{e}_\phi$	unit vectors of cylindrical coordinate system
$\mathbf{e}_\xi, \mathbf{e}_\beta, \mathbf{e}_n$	unit vectors of curvilinear coordinate system

f	shock radius (eq. (1)), nondimensionalized by L
g	metrics of curvilinear coordinate system (see appendix A)
h_ξ, h_β, h_n	scale factors of curvilinear coordinate system, nondimensionalized by L
J	Jacobian of coordinate transformation
L	reference length
M	Mach number
n	coordinate in normal direction, nondimensionalized by L
$\mathbf{P}$	position vector from origin of coordinate system
p	static pressure, nondimensionalized by $\rho_\infty V_\infty^2$
R	radius of curvature, nondimensionalized by L
r	radius in cylindrical coordinate system, nondimensionalized by L
u, v, w	velocity components of curvilinear coordinate system, nondimensionalized by V_∞
V	velocity magnitude
$\mathbf{V}$	velocity vector, nondimensionalized by V_∞
x, y, z	Cartesian coordinate system referenced to shock or body, nondimensionalized by L
α	angle of attack
$\beta, \overline{\beta}$	coordinate perpendicular to shockline and unit normal vector, nondimensionalized by L
Γ	shock-wave angle relative to free-stream velocity (see fig. 1)
δ_ϕ	shock-wave angle in circumferential direction (see fig. 1)
ϵ	axial distance from origin at which integration of shock variables is started
η	ratio of stream function ψ to its value on shock
θ	inclination angle of body surface with respect to body axis
$\xi, \overline{\xi}$	curvilinear coordinates along shock line, nondimensionalized by L
ρ	density, nondimensionalized by ρ_∞
σ	shock-wave angle, $\phi - \delta_\phi$
Φ, ψ	stream functions (eq. (9)), nondimensionalized by $\rho_\infty V_\infty L^2$
ϕ	cylindrical coordinate (see fig. 1)

Subscripts:

b	value on body
c	property on conical afterbody of spherically blunted cone
i	conic-section parameters specific to ϕ = Constant plane
j	marching step
s	value on shock surface
∞	free-stream conditions

Analysis

Coordinate Systems

For a three-dimensional shock wave, a cylindrical coordinate system (x, r, ϕ) is used, and the x-axis is aligned with the free-stream velocity vector. The shock-wave geometry (ref. 19) may be described by

$$r_s = f(x, \phi) \tag{1}$$

Two angles that define the shock-wave shape are

$$\tan \delta_\phi = \frac{1}{f} \frac{\partial f}{\partial \phi} \tag{2}$$

$$\tan \Gamma = \frac{\partial f}{\partial x} \cos \delta_\phi \tag{3}$$

A third angle is given by the relation

$$\sigma = \phi - \delta_\phi \tag{4}$$

All three angles are shown in figure 1. For the special case of axisymmetric flow, $\Gamma = \Gamma(x)$, $\delta_\phi = 0$, and $\sigma = \phi$.

Next a shock-oriented curvilinear coordinate system (ξ, β, n) is defined with corresponding unit vectors $(\mathbf{e}_\xi, \mathbf{e}_\beta, \mathbf{e}_n)$ and velocities (u, w, v). This coordinate system (refs. 1 and 20) is appropriate for hypersonic flow ($M_\infty >> 1$) and thin shock layers. The unit vector $\mathbf{e}_{ns}$ is the inward vector normal to the shock surface. The coordinates ξ and β are chosen such that $\mathbf{e}_{\xi s}$ is in the direction of the tangential velocity component just inside the shock surface. The unit vector $\mathbf{e}_{\beta s}$ is perpendicular to $\mathbf{e}_{\xi s}$ and $\mathbf{e}_{ns}$. (See fig. 2.) This coordinate system is defined as orthogonal at the shock surface but is nonorthogonal in the shock layer for a general three-dimensional shock. The derivations of the unit vectors and the metrics in the shock layer are outlined in appendix A.

The postshock relations can be written as

$$\begin{aligned} \mathbf{V}_s &= u_s \mathbf{e}_{\xi s} + v_s \mathbf{e}_{ns} \\ w_s &= 0 \end{aligned} \tag{5}$$

whereas in general, through the shock layer,

$$\mathbf{V} = u\mathbf{e}_\xi + v\mathbf{e}_n + w\mathbf{e}_\beta \tag{6}$$

The component of the free-stream velocity tangent to the shock wave is unchanged across the shock wave; therefore, the unit vectors $\mathbf{e}_\xi, \mathbf{e}_\beta$, and $\mathbf{e}_n$ at the shock are

$$\left.\begin{aligned} \mathbf{e}_{\xi s} &= \cos\Gamma \mathbf{e}_x + \sin\Gamma\,(\cos\delta_\phi \mathbf{e}_r - \sin\delta_\phi \mathbf{e}_\phi) \\ \mathbf{e}_{\beta s} &= \sin\delta_\phi \mathbf{e}_r + \cos\delta_\phi \mathbf{e}_\phi \\ \mathbf{e}_{ns} &= \sin\Gamma \mathbf{e}_x - \cos\Gamma\,(\cos\delta_\phi \mathbf{e}_r - \sin\delta_\phi \mathbf{e}_\phi) \end{aligned}\right\} \tag{7}$$

The differential arc lengths along each coordinate direction at the shock are $h_{\xi s}\, d\xi$, $h_{\beta s}\, d\beta$, and $h_{ns}\, dn$, respectively. The scale factors $h_{\xi s}, h_{\beta s}$, and h_{ns} govern the stretching of the corresponding coordinates. The scale factor in the n-direction h_{ns} is unity, since it is a straight-line distance.

Governing Equations

Stream functions. The continuity equation for three-dimensional flows given by

$$\nabla \cdot (\rho \mathbf{V}) = 0 \tag{8}$$

is satisfied by two stream functions. The continuity equation can be written as

$$\rho \mathbf{V} = \nabla\psi \times \nabla\Phi \tag{9}$$

where ψ and Φ represent the two stream functions (ref. 16).

As noted in references 13 and 16 for blunt bodies at hypersonic speeds, most of the mass flow is near the shock wave, where the velocity component w is small. A simplifying assumption is made in this study that $w = 0$ throughout the shock layer. Thus, if Φ is set equal to β, ψ becomes

$$\frac{\partial\psi}{\partial n} = \frac{\rho u J}{h_\xi} \tag{10}$$

$$\frac{\partial\psi}{\partial\xi} = \rho v J \tag{11}$$

where J represents the Jacobian of transformation from (ξ, β, n) to (x, y, z) and is given by

$$J = h_{\xi s} h_{\beta s} \left[\left(1 - n\frac{1}{R}\right) \left(1 - n\cos\Gamma \frac{1}{h_{\beta s}} \frac{\partial\sigma}{\partial\beta}\right) - \left(n \frac{1}{h_{\beta s}} \frac{\partial\Gamma}{\partial\beta}\right)^2 \right] \tag{12}$$

These definitions of ψ and Φ are not unique, and they satisfy the exact flow-field equations only at the shock wave. The intersections of β = Constant planes with the shock surface are referred to as shock lines. Shock lines are in the direction of the ξ-coordinate, and for axisymmetric flow, β = Constant planes are meridional planes.

Pressure equation. The momentum equations for steady, inviscid flow may be written as

$$\rho(\mathbf{V} \cdot \nabla\mathbf{V}) + \nabla p = 0 \tag{13}$$

Writing these equations in the ξ, β, n system gives the following momentum equation normal to the shock:

$$\frac{u}{h_\xi}\frac{\partial v}{\partial \xi} + v\frac{\partial v}{\partial n} + u^2\left(\frac{h_{\xi s}}{h_\xi}\right)^2\left[\left(1 - n\frac{1}{R}\right)\frac{1}{R} - n\left(\frac{1}{h_{\beta s}}\frac{\partial \Gamma}{\partial \beta}\right)^2\right] + \frac{1}{\rho}\frac{\partial p}{\partial n} = 0 \tag{14}$$

where R is the radius of curvature of the shock in the ξ-n plane. Transforming this equation from the ξ, β, n system to a new set of independent variables $(\bar{\xi}, \bar{\beta}, \eta)$ by using equations (10) and (11) gives

$$\frac{\partial p}{\partial \eta} = \frac{\psi_s}{J}\left\{\frac{\partial v}{\partial \bar{\xi}} + u\left(\frac{h_{\xi s}^2}{h_\xi}\right)\left[\left(1 - n\frac{1}{R}\right)\frac{1}{R} - n\left(\frac{1}{h_{\beta s}}\frac{\partial \Gamma}{\partial \beta}\right)^2\right]\right\} - \frac{h_{\xi s} h_{\beta s}\eta \sin\Gamma}{J}\frac{\partial v}{\partial \eta} \tag{15}$$

where

$$\bar{\xi} = \xi$$

$$\bar{\beta} = \beta$$

$$\eta = \psi/\psi_s$$

Note that $\eta = 1$ on the shock and $\eta = 0$ on the body surface. From the transformation, an expression for the velocity component v normal to the shock can be obtained and is given by

$$v = \frac{u}{h_\xi}\frac{\partial n}{\partial \bar{\xi}} + \frac{h_{\xi s} h_{\beta s}\eta \sin\Gamma}{\rho J} \tag{16}$$

The only assumption used in equations (15) and (16) is that the velocity component w is equal to zero throughout the shock layer. However, to obtain explicit expressions for the pressure and normal velocity component, additional assumptions are required. The following approximations, which are consistent with the simplifications in references 13 and 16, are valid for hypersonic flow ($M_\infty >> 1$) and thin shock layers:

$$n \approx \left(\frac{\partial n}{\partial \eta}\right)_s (\eta - 1)$$

$$\frac{\partial \rho_s}{\partial \bar{\xi}} \approx 0$$

$$\rho \approx \rho_s$$

$$u \approx u_s$$

$$\frac{h_{\xi s}}{h_\xi} \approx 1$$

$$J \approx h_{\xi s} h_{\beta s}$$

$$\frac{\partial v}{\partial \bar{\xi}} \approx 0$$

Equations (15) and (16) can now be simplified as

$$p\left(\bar{\xi}, \bar{\beta}, \eta\right) = p_s\left(\bar{\xi}, \bar{\beta}\right) + \frac{u_s \psi_s}{R h_{\beta s}}(\eta - 1) - \frac{v_s \psi_s \tan\Gamma}{h_{\beta s}}\left(\frac{1}{R} + \cos\Gamma \frac{1}{h_{\beta s}}\frac{\partial \sigma}{\partial \beta}\right)\frac{\eta^2 - 1}{2} \tag{17}$$

and

$$v(\overline{\xi},\overline{\beta},\eta) = v_s\left(\overline{\xi},\overline{\beta}\right)\left[1+\frac{\psi_s}{h_{\beta s}\cos\Gamma}\left(\frac{1}{R}+\cos\Gamma\frac{1}{h_{\beta s}}\frac{\partial\sigma}{\partial\beta}\right)(\eta-1)\right] \tag{18}$$

If $h_{\beta s} = r_s$, equation (17) becomes Maslen's second-order pressure equation for axisymmetric flow. (See ref. 16.) The pressure and normal component of velocity can now be found explicitly along a line normal to the shock surface, since all variables in equations (17) and (18) are evaluated on the shock. The surface pressure is easily found, since the stream function ψ and, thus, η are zero on the body. Equations (17) and (18) are approximate.

Other relations. The energy equation for steady, adiabatic, inviscid flow reduces to the simple relation that the total enthalpy of the flow is constant. Also, for inviscid equilibrium or frozen flow, the (postshock) entropy is constant along a streamline. With these two relations, the density and streamwise component of velocity u can be computed. (See fig. 3.) The distance from the shock surface to the body along a line normal to the shock is calculated by integrating equation (10) and noting that the Jacobian and scale factors are functions of the distance n as outlined in appendix A.

These relations for pressure, density, the two velocity components, and shock-layer thickness outline an inverse method of solution in which the shock shape (not the body shape) is known. Therefore, the shock shape must be changed until the correct body shape is produced. The resulting iteration procedure is handled differently in each region of the flow.

Method of Solution

In the stagnation region of a blunt body traveling at hypersonic speeds, the flow is subsonic. Because of the elliptic behavior of the flow-field equations in this region, a marching scheme is not well posed. Thus, the complete shock shape for the entire subsonic-transonic region must be determined iteratively. A marching procedure is then used downstream of the subsonic-transonic region, where the flow is completely supersonic.

Subsonic-transonic region. In this investigation, the blunt-nose region of the body in a body-oriented coordinate system is represented by a longitudinal conic section with an elliptical cross section as

$$B_b y_b^2 + z_b^2 = 2R_b x_b - b_b x_b^2 \tag{19}$$

where R_b is the nose radius of the body in the x_b-z_b plane relative to the principal shock radius of curvature in the x-z plane, b_b determines the longitudinal shape of the body, and B_b governs the ellipticity of the body cross section. Van Dyke and Gordon (ref. 21) suggested that a conic-section body shape produces a shock surface that can also be described by a conic section. This assumption is used in the present analysis. Since a three-dimensional shock needs to be specified, longitudinal conic sections are blended in the circumferential direction by using one or more elliptical arcs to produce the shock surface in the subsonic region. One advantage to this approach is that parameters are easily added by blending more conic sections.

The equation of the longitudinal (ϕ = Constant) conic sections is given by

$$r_s^2 + b_i x_s^2 - 2c_i x_s + d_i x_s r_s = 0 \tag{20}$$

where b_i, c_i, and d_i are parameters local to a plane where ϕ is constant in the wind-oriented system. At each x-location on the shock, the radii that are determined from equation (20) in each meridional plane are fitted with one or more elliptical segments to produce the circumferential variation of the shock radius. The number of parameters (b_i, c_i, and d_i) to calculate then depends on the number of planes. In this report, only three planes ($\phi = 0$, $\phi = \pi/2$, and $\phi = \pi$) are blended by using one cross-sectional ellipse to give a shock surface in the nose region. This method is adequate for axisymmetric shapes at angle of attack and for bodies with elliptical cross sections at moderate angles of attack. However, for elliptical bodies at larger angles of attack, more parameters and more elliptical segments may be needed to accurately describe the shock surface.

In the iteration procedure, the shock shape is first assumed to be equal to the body shape, and the conic-section parameters for the shock are chosen accordingly. Next, the shock standoff distance is computed from the limiting form of the shock-layer equations on the stagnation line. (See ref. 1.) Shock lines are then traced from the stagnation region to the sonic surface by integrating the following differential equations that govern the shock shape along a shock line (β = Constant):

$$\frac{\partial r_s}{\partial x} = \tan\Gamma\cos\delta_\phi \tag{21}$$

$$\frac{\partial \phi_s}{\partial x} = -\frac{\tan\Gamma \sin\delta_\phi}{r_s} \tag{22}$$

$$\frac{\partial \psi_s}{\partial x} = h_{\beta s} \tan\Gamma \tag{23}$$

$$\frac{\partial h_{\beta s}}{\partial x} = \tan\Gamma \frac{\partial \sigma}{\partial \beta} \tag{24}$$

$$\frac{\partial \sin\Gamma}{\partial x} = -\frac{1}{R} \tag{25}$$

where x is the independent axial coordinate. The shock variables are integrated along each shock line with a variable-step-size, third-order, predictor-corrector, ordinary differential-equation solver. Angles and derivatives are determined by blending the longitudinal conic sections. The transformation operators used in the development of these equations are derived in appendix B. Since these equations are indeterminate at the stagnation line ($x_s = 0$), the integration begins a small distance ϵ from the origin (ref. 19). At $x_s = \epsilon$, the coordinate ϕ_s is assumed to be equal to the curvilinear coordinate β.

The approximate shock-layer equations for pressure, density, velocity, and shock-layer thickness are used to calculate the position of the body at discrete locations. These points are placed primarily near the end of the subsonic-transonic region, where a good starting solution is crucial to the downstream marching procedure. The error between the geometric and calculated distance from the shock to the body is used to change the parameters of the shock surface in a quasi-Newton nonlinear equations solver. If the number of parameters is less than the number of calculated body points, the shock is determined in a least-squares sense. However, improved results downstream are obtained if the points on the body surface are matched exactly. Because three planes are used in this report, a total of nine parameters are varied until nine points on the body have the correct shock-layer thickness.

Supersonic region. Once past the transonic region, the flow is totally supersonic and a marching scheme is well posed. The shock surface and resulting shock lines from the transonic region form a starting solution for the marching procedure.

The differential equations that govern the shock shape along a shock line are given by equations (21) to (25). However, in the supersonic region, δ_ϕ and $\partial\sigma/\partial\beta$ are computed from finite differences in the circumferential direction at each x-location.

The general marching procedure is outlined here. Starting at x_j, predicted values for the shock variables ($r_s, \phi_s, \psi_s, h_{\beta s}$, and Γ_s) are obtained at x_{j+1} for each shock line. The angle δ_ϕ and the derivative $\partial\sigma/\partial\beta$ are computed from finite differences by using the predicted values of the shock radius. On each shock line, the local shock curvature $1/R$ is varied in the approximate shock-layer equations that govern pressure, density, velocity, and shock-layer thickness until the calculated thickness matches the geometric shock-layer thickness. Convergence usually required two or three iterations with the secant method. These values of the shock curvature are now used to determine corrected values of the shock variables at x_{j+1} for each shock line. Updated values for δ_ϕ, $\partial\sigma/\partial\beta$, and $1/R$ are calculated in the same fashion as in the predictor step. Upon completion of the corrector step at x_{j+1} for each shock line, predicted values for the shock variables are obtained at x_{j+2}, and the entire process is repeated.

Results and Discussion

Results at perfect-gas conditions are presented for this investigation over a spherically blunted cone, a paraboloid, and an elliptical cone at angle of attack. Solutions are described in a body-oriented coordinate system with the circumferential angle ϕ_b equal to 0° in the windward plane of symmetry and 180° along the leeward ray. Distances are referenced to the nose radius of the body. Nondimensional pressures are obtained by dividing by $\rho_\infty V_\infty^2$.

Surface pressures obtained with the present technique for a spherically blunted circular cone at 0° angle of attack are shown in figures 4 and 5. The cone half-angle is 10° for both cases, and the free-stream Mach numbers are 5 and 20, respectively. Comparisons with a finite-difference solution (ref. 7) of the inviscid-flow equations show excellent agreement with the higher Mach number results of the present method. Comparisons of the detailed and present results at the lower Mach number condition are good. The discrepancies at this condition may be the results of shock-layer approximations used in the present method.

The pressure distribution over the 10° blunted cone at an angle of attack of 10° is shown in figure 6. The solution in the wind axes over the spherical nose at angle of attack is identical to the nose solution over a sphere at 0° angle of attack if the subsonic-transonic region remains on the spherical cap. The surface pressures along the windward ray again compare favorably with the predicted values of reference 7. However, in the leeward plane, the present technique underpredicts the Naval Surface

Weapons Center (NSWC) surface pressure by an average of 10 percent. The circumferential pressure distribution in figure 7, the shock shape in the planes of symmetry in figure 8, and the pressure profiles in figures 9 and 10 confirm the high degree of accuracy of the technique in the region of the windward plane.

Shock shapes and surface pressures for a paraboloid at 8° angle of attack are presented in figures 11 to 13. Experimental results are presented at free-stream Mach numbers of 9.9 for the surface pressures and 5.73 for the shock shape. Although a paraboloid is axisymmetric, the shock shape produced in the nose region is fully three-dimensional when the body is at angle of attack. This comparison is a more significant test of the capabilities of the iteration procedure in the subsonic-transonic region than for the spherically blunted cones at angle of attack, because in the wind axes, the flow is no longer axisymmetric. For the paraboloid at angle of attack, three longitudinal conic sections were blended by using a cross-sectional ellipse to produce the shock shape in the nose region. Six iterations using the quasi-Newton nonlinear equations solver were required for convergence. Good agreement (within 8 percent) in surface pressures between the present method and the experimental data (ref. 22) is shown in figures 11 and 12. In figure 13, the calculated shock lies slightly closer to the body than does the experimentally determined shock shape, but the agreement is good. Comparisons in reference 22 at 0° angle of attack were made with the axisymmetric Maslen technique of Zoby and Graves (ref. 14), and a similar result was observed.

Surface pressures over an elliptical cone with a cone half-angle of 10.26° in the windward plane and an ellipticity of 1.5 are shown in figures 14 and 15 at a free-stream Mach number of 10. The experimental data (ref. 23) displayed are for a pointed elliptical cone. Since the present method currently allows for blunted bodies only, a very small bluntness is assumed for the elliptical cone. Circumferential pressures are shown for a position far downstream ($x/R_b = 120$), where the surface pressures should approach sharp cone values. As in the case of a spherically blunted cone at angle of attack, the surface pressures on the elliptical cone at 10° angle of attack show excellent agreement with the experimental data near the windward plane, but they diverge as the leeward ray is approached. However, viscous effects are more pronounced in the leeward plane, and an inviscid method is not appropriate for calculations in this region.

To estimate the relative computing times of the present technique and more exact methods that numerically solve the full inviscid equations, the present method and the Euler equation solver given in reference 7 were run on a CDC® Cyber 170 computer and run times were compared. Solutions over spherically blunted cones with cone half-angles of 5° and 10° and lengths from 50 to 100 nose radii were computed for angles of attack of 0° to 10°. The Mach number for all cases was 10. Based on these comparisons, the present method is consistently five times faster per meridional plane than the Euler code of reference 7. For a 10° cone at 10° angle of attack, and for a length of 50 nose radii, the Euler code requires 150 CPU sec of computer time, while the present technique requires 30 sec. Nine meridional planes were used in the Euler code, and a corresponding number of shock lines were used in the present method.

Solutions were also computed over the nose region of a blunt elliptical cone with an ellipticity of 1.5 using the present method and the time-dependent Euler solver code HALIS (High Alpha Inviscid Solution) of reference 4. Both methods were run on a Cray-2 S supercomputer, and run times were compared. For a length of 0.75 nose radii and a free-stream Mach number of 10, HALIS requires 120 CPU sec, while the present technique requires less than 1 CPU sec. Surface pressure distributions in the planes of symmetry are presented in figure 16. The circumferential pressure distribution at an axial location of 0.4 nose radii is shown in figure 17, and there is excellent agreement between the present method and HALIS. These comparisons indicate that the present technique may be much faster than more exact CFD methods for 3-D nose shapes.

The present approximate 3-D inviscid method has been shown to produce pressure profiles and surface distributions and corresponding shock shapes that are in good agreement with detailed predictions and experimental data. The procedure significantly improves the current engineering capability of predicting inviscid flow fields over 3-D surfaces. The present inviscid technique may be coupled with the aeroheating prediction method described in reference 1 to calculate heating rates near the windward plane of symmetry on reentry vehicles. The speed of the present method allows it to be easily run on a computer workstation; therefore, it is ideal in a design environment.

Concluding Remarks

An approximate technique has been developed that determines the flow field over blunt-nose bodies at hypersonic speeds. An explicit expression from Maslen for the pressure across the shock layer and the assumption of approximate stream surfaces in the shock layer are used to simplify the three-dimensional flow. The method is applied to the solution over

spherically blunted cones, paraboloids, and elliptical cones at angle of attack for a perfect gas.

The present technique predicts shock surfaces and shock-layer properties that compare favorably with the more exact numerical solutions and experimental results. Excellent agreement is obtained near the windward plane of symmetry. The method is also very rapid when compared with the more exact finite-difference solutions of the inviscid equations, in particular the solution over three-dimensional (3-D) bodies. Therefore, this technique is especially attractive for engineering aeroheating methods that require inviscid hypersonic flow-field information.

NASA Langley Research Center
Hampton, VA 23665-5225
July 11, 1990

Appendix A

Variation of Unit Vectors and Metrics Across Shock Layer

If $\mathbf{P}_s$ is the position vector, relative to the origin, for a point on the shock wave and $\mathbf{P}$ is a position vector for a point normal to the shock wave at $\mathbf{P}_s$, then

$$\mathbf{P}(\xi, \beta, n) = \mathbf{P}_s(\xi, \beta) + n\mathbf{e}_{ns}(\xi, \beta) \tag{A1}$$

The coordinate directions in the shock layer are found from the following equations:

$$\left.\begin{aligned} \mathbf{e}_\xi &= \frac{\partial \mathbf{P}}{\partial \xi} \\ \mathbf{e}_\beta &= \frac{\partial \mathbf{P}}{\partial \beta} \\ \mathbf{e}_n &= \frac{\partial \mathbf{P}}{\partial n} \end{aligned}\right\} \tag{A2}$$

Differentiating equation (A1) and substituting into equation (A2), using the definition of the unit vectors at the shock (eq. (7)), yields

$$\left.\begin{aligned} \mathbf{e}_\xi &= h_{\xi s}\left[\left(1 - n\frac{1}{R}\right)\mathbf{e}_{\xi s} + n\frac{1}{h_{\beta s}}\frac{\partial \Gamma}{\partial \beta}\mathbf{e}_{\beta s}\right] \\ \mathbf{e}_\beta &= h_{\beta s}\left[n\frac{1}{h_{\beta s}}\frac{\partial \Gamma}{\partial \beta}\mathbf{e}_{\xi s} + \left(1 - n\cos\Gamma\frac{1}{h_{\beta s}}\frac{\partial \sigma}{\partial \beta}\right)\mathbf{e}_{\beta s}\right] \\ \mathbf{e}_n &= \mathbf{e}_{ns} \end{aligned}\right\} \tag{A3}$$

where

$$\frac{1}{R} = -\frac{1}{h_{\xi s}}\frac{\partial \Gamma}{\partial \xi}$$

$$\frac{1}{h_{\beta s}}\frac{\partial \Gamma}{\partial \beta} = -\frac{\cos\Gamma}{h_{\xi s}}\frac{\partial \sigma}{\partial \xi}$$

The metrics for a nonorthogonal coordinate system are given by

$$g_{ij} = \mathbf{e}_i \cdot \mathbf{e}_j \tag{A4}$$

where i and j are indices that represent the coordinates ξ, β, and n. Therefore,

$$\left.\begin{aligned} g_{\xi\xi} &= h_{\xi s}^2 \left[\left(1 - n\frac{1}{R}\right)^2 + \left(n\frac{1}{h_{\beta s}}\frac{\partial \Gamma}{\partial \beta}\right)^2 \right] \\ g_{\beta\beta} &= h_{\beta s}^2 \left[\left(1 - n\cos\Gamma\frac{1}{h_{\beta s}}\frac{\partial \sigma}{\partial \beta}\right)^2 + \left(n\frac{1}{h_{\beta s}}\frac{\partial \Gamma}{\partial \beta}\right)^2 \right] \\ g_{nn} &= 1 \\ g_{\xi\beta} &= g_{\beta\xi} = h_{\xi s} h_{\beta s} \left(n\frac{1}{h_{\beta s}}\frac{\partial \Gamma}{\partial \beta}\right) \left[\left(1 - n\frac{1}{R}\right) + \left(1 - n\cos\Gamma\frac{1}{h_{\beta s}}\frac{\partial \sigma}{\partial \beta}\right) \right] \\ g_{\xi n} &= g_{n\xi} = 0 \\ g_{\beta n} &= g_{n\beta} = 0 \end{aligned}\right\} \tag{A5}$$

The Jacobian of transformation from (ξ, β, n) to (x, y, z) is given by

$$J = |g_{ij}|^{1/2} = h_{\xi s} h_{\beta s} \left[\left(1 - n\frac{1}{R}\right) \left(1 - n\cos\Gamma\frac{1}{h_{\beta s}}\frac{\partial \sigma}{\partial \beta}\right) - \left(n\frac{1}{h_{\beta s}}\frac{\partial \Gamma}{\partial \beta}\right)^2 \right] \tag{A6}$$

The scale factors are defined to be the magnitudes of the vectors and are therefore

$$\left.\begin{aligned} h_\xi &= (g_{\xi\xi})^{1/2} \\ h_\beta &= (g_{\beta\beta})^{1/2} \\ h_n &= (g_{nn})^{1/2} = 1 \end{aligned}\right\} \tag{A7}$$

Appendix B

Transformation Operators at Shock Surface

The unit vectors at the shock in the curvilinear coordinate system (ξ, β, n) are

$$\left.\begin{aligned} \mathbf{e}_{\xi s} &= \cos\Gamma \mathbf{e}_x + \sin\Gamma(\cos\delta_\phi \mathbf{e}_r - \sin\delta_\phi \mathbf{e}_\phi) \\ \mathbf{e}_{\beta s} &= \sin\delta_\phi \mathbf{e}_r + \cos\delta_\phi \mathbf{e}_\phi \\ \mathbf{e}_{ns} &= \sin\Gamma \mathbf{e}_x - \cos\Gamma(\cos\delta_\phi \mathbf{e}_r - \sin\delta_\phi \mathbf{e}_\phi) \end{aligned}\right\} \tag{B1}$$

If the transformation operators are derived for the curvilinear system with respect to the cylindrical coordinates and a position vector $\mathbf{P}_s$ on the shock surface is defined, the vector may be expressed as

$$\mathbf{P}_s = x\mathbf{e}_x + f\mathbf{e}_r \tag{B2}$$

where

$$r_s = f(x, \phi)$$

The derivative of this vector is

$$d\mathbf{P}_s = \left(\mathbf{e}_x + \frac{\partial f}{\partial x}\mathbf{e}_r\right)\, dx + \left(\mathbf{e}_\phi + \frac{1}{f}\frac{\partial f}{\partial \phi}\mathbf{e}_r\right) f\, d\phi \tag{B3}$$

In curvilinear coordinates, equation (B3) becomes

$$d\mathbf{P}_s = \frac{\partial \mathbf{P}_s}{\partial \xi}\, d\xi + \frac{\partial \mathbf{P}_s}{\partial \beta}\, d\beta = \mathbf{e}_{\xi s} h_{\xi s}\, d\xi + \mathbf{e}_{\beta s} h_{\beta s}\, d\beta \tag{B4}$$

Using equations (B3) and (B4) and taking the dot product with $\mathbf{e}_x$ gives

$$dx = \mathbf{e}_{\xi s} \cdot \mathbf{e}_x h_{\xi s}\, d\xi + \mathbf{e}_{\beta s} \cdot \mathbf{e}_x h_{\beta s}\, d\beta = \frac{\partial x}{\partial \xi}\, d\xi + \frac{\partial x}{\partial \beta}\, d\beta \tag{B5}$$

This process yields

$$\left.\begin{aligned} \frac{\partial x}{\partial \xi} &= \mathbf{e}_{\xi s} \cdot \mathbf{e}_x h_{\xi s} \\ \frac{\partial x}{\partial \beta} &= \mathbf{e}_{\beta s} \cdot \mathbf{e}_x h_{\beta s} \end{aligned}\right\} \tag{B6}$$

Taking the dot product of equations (B3) and (B4) with respect to ϕ gives

$$\left.\begin{aligned} \frac{\partial \phi}{\partial \xi} &= \frac{\mathbf{e}_{\xi s} \cdot \mathbf{e}_\phi}{f} h_{\xi s} \\ \frac{\partial \phi}{\partial \beta} &= \frac{\mathbf{e}_{\beta s} \cdot \mathbf{e}_\phi}{f} h_{\beta s} \end{aligned}\right\} \tag{B7}$$

The transformation operators at the shock may now be written, using equations (B1), (B6), and (B7) as

$$\left.\begin{aligned} \frac{1}{h_{\xi s}}\frac{\partial}{\partial \xi} &= \cos\Gamma \frac{\partial}{\partial x} - \frac{\sin\Gamma \sin\delta_\phi}{r_s}\frac{\partial}{\partial \phi} \\ \frac{1}{h_{\beta s}}\frac{\partial}{\partial \beta} &= \frac{\cos\delta_\phi}{r_s}\frac{\partial}{\partial \phi} \end{aligned}\right\} \tag{B8}$$

References

1. DeJarnette, Fred R.; and Hamilton, H. Harris: Aerodynamic Heating on 3-D Bodies Including the Effects of Entropy-Layer Swallowing. *J. Spacecr. & Rockets,* vol. 12, no. 1, Jan. 1975, pp. 5–12.
2. Zoby, E. V.; and Simmonds, A. L.: Engineering Flowfield Method With Angle-of-Attack Applications. *J. Spacecr. & Rockets,* vol. 22, July–Aug. 1985, pp. 398–405.
3. Hamilton, H. Harris, II: *Calculation of Laminar Heating Rates on Three-Dimensional Configurations Using the Axisymmetric Analogue.* NASA TP-1698, 1980.
4. Weilmuenster, K. James; and Hamilton, H. Harris, II (appendix C by M. J. Hamilton): *Calculations of Inviscid Flow Over Shuttle-Like Vehicles at High Angles of Attack and Comparisons With Experimental Data.* NASA TP-2103, 1983.
5. Weilmuenster, K.; Smith, R.; and Greene, F.: Assured Crew Return Vehicle Flowfield and Aerodynamic Characteristics. AIAA-90-0229, Jan. 1990, p. 15.
6. Marconi, Frank; Salas, Manuel; and Yaeger, Larry: *Development of a Computer Code for Calculating the Steady Super/Hypersonic Inviscid Flow Around Real Configurations. Volume I—Computational Technique.* NASA CR-2675, 1976.
7. Morrison, A. M.; Solomon, J. M.; Ciment, M.; Ferguson, R. E.: *Handbook of Inviscid Sphere-Cone Flow Fields and Pressure Distributions—Volume 1,* NSWC/WOL/TR-75-45, Vol. 1, U.S. Navy, Dec. 1, 1975. (Available from DTIC as AD A021 960.)
8. Gnoffo, Peter A.: *An Upwind-Biased, Point-Implicit Relaxation Algorithm for Viscous, Compressible Perfect-Gas Flows.* NASA TP-2953, 1990.
9. Lawrence, S. L.; Chaussee, D. S.; and Tannehill, J. C.: Application of an Upwind Algorithm to the Three-Dimensional Parabolized Navier-Stokes Equations. AIAA-87-1112-CP, June 1987.
10. Murray, Alvin L.; and Lewis, Clark H.: Hypersonic Three-Dimensional Viscous Shock-Layer Flows Over Blunt Bodies. *AIAA J.,* vol. 16, no. 12, Dec. 1978, pp. 1279–1286.
11. Thereja, R. R.; Szema, K. Y.; and Lewis, C. H.: Chemical Equilibrium Laminar or Turbulent Three-Dimensional Viscous Shock-Layer Flows. *J. Spacecr. & Rockets,* vol. 20, no. 5, Sept.–Oct. 1983, pp. 454–460.
12. Swaminathann, S.; Kim, M. D.; and Lewis, C. H.: Three-Dimensional Nonequilibrium Viscous Shock-Layer Flows Over Complex Geometries. AIAA-83-0212, Jan. 1983.
13. Maslen, S. H.: Inviscid Hypersonic Flow Past Smooth Symmetric Bodies. *AIAA J.,* vol. 2, no. 6, June 1964, pp. 1055–1061.
14. Zoby, Ernest V.; and Graves, Randolph A., Jr.: *A Computer Program for Calculating the Perfect Gas Inviscid Flow Field About Blunt Axisymmetric Bodies at an Angle of Attack of 0°.* NASA TM X-2843, 1973.
15. Jackson, Sherman Keith, Jr.: The Viscous-Inviscid Hypersonic Flow of a Perfect Gas Over Smooth Symmetric Bodies. Ph.D. Thesis, Univ. of Colorado, 1966.
16. Maslen, Stephen H.: *Asymmetric Hypersonic Flow.* NASA CR-2123, 1972.
17. Maslen, Stephen H.: *Development of a Method of Analysis and Computer Program for Calculating the Inviscid Flow About the Windward Surfaces of Space Shuttle Configurations at Large Angles of Attack.* NASA CR-132453, 1974.
18. Maslen, S. H.: *Inviscid Flow About Blunted Cones of Large Opening Angle at Angle of Attack.* NASA CR-132652, 1975.
19. DeJarnette, Fred R.; and Hamilton, H. Harris: Inviscid Surface Streamlines and Heat Transfer on Shuttle-Type Configurations. *J. Spacecr. & Rockets,* vol. 10, no. 6, May 1973, pp. 314–321.
20. Riley, Christopher J.: An Approximate Method for Calculating Inviscid Flow Fields Over Three-Dimensional Blunt-Nosed Bodies in Hypersonic Flow. M.S. Thesis, North Carolina State University, 1988.
21. Van Dyke, Milton D.; and Gordon, Helen D.: *Supersonic Flow Past a Family of Blunt Axisymmetric Bodies.* NASA TR R-1, 1959.
22. Miller, Charles G., III: *Measured Pressure Distributions, Aerodynamic Coefficients, and Shock Shapes on Blunt Bodies at Incidence in Hypersonic Air and CF_4.* NASA TM-84489, 1982.
23. Palko, R. L.; and Ray, A. D.: *Pressure Distribution and Flow Visualization Tests of a 1.5 Elliptic Cone at Mach 10.* AEDC-TDR-63-163, U.S. Air Force, Aug. 1963.

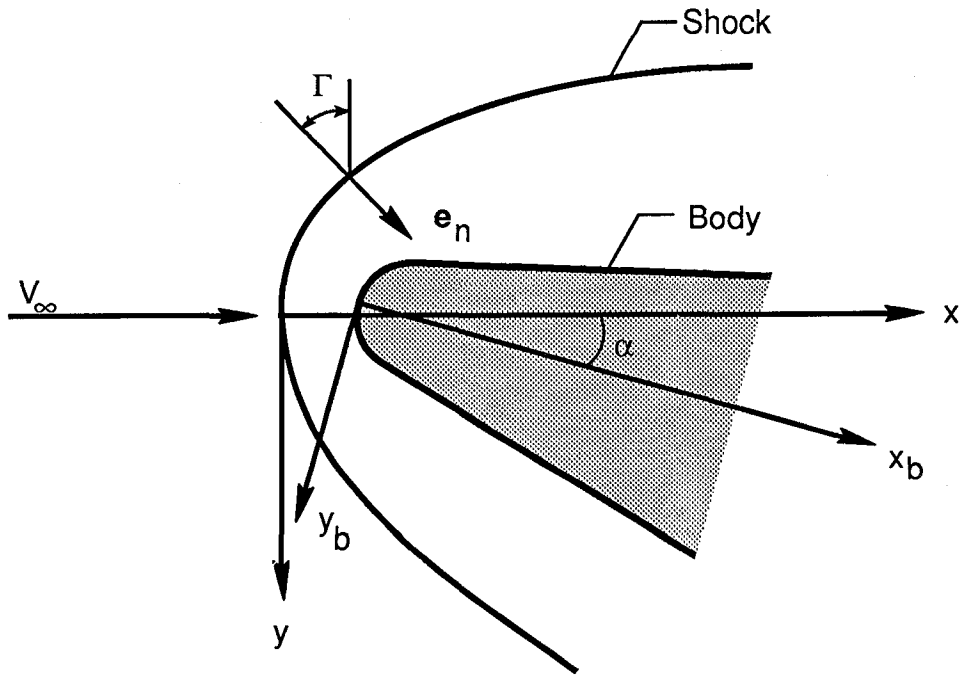

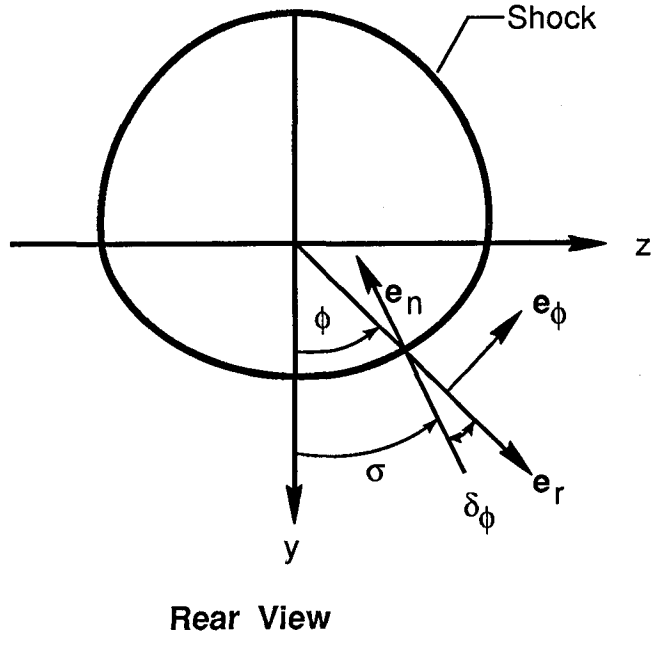

Figure 1. Shock wave and body geometry.

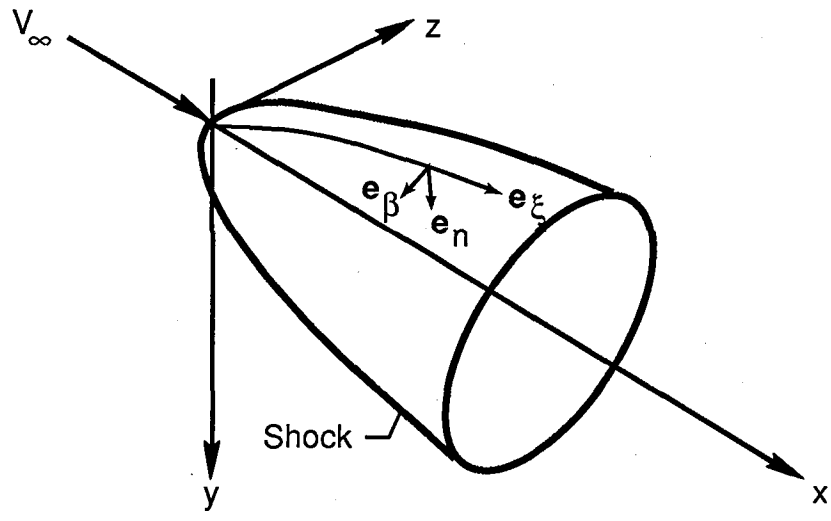

Isometric View

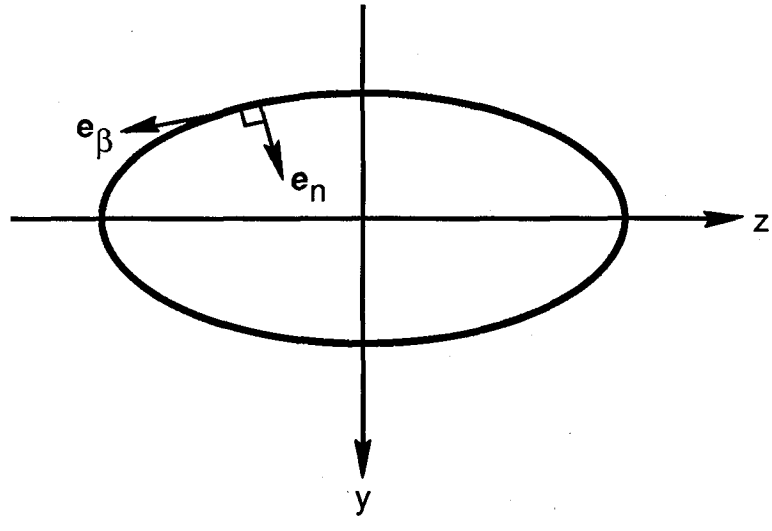

Rear View

Figure 2. Shock-oriented curvilinear coordinate system.

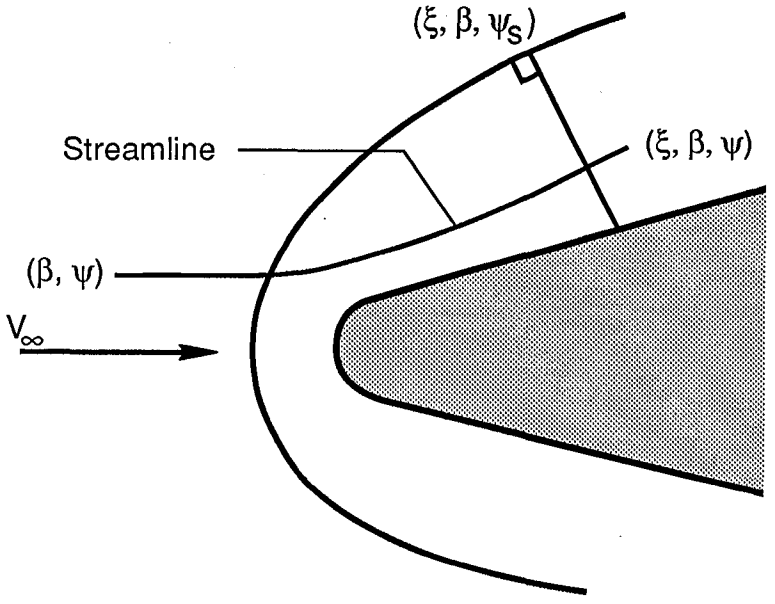

Figure 3. Coordinate positions (β = Constant).

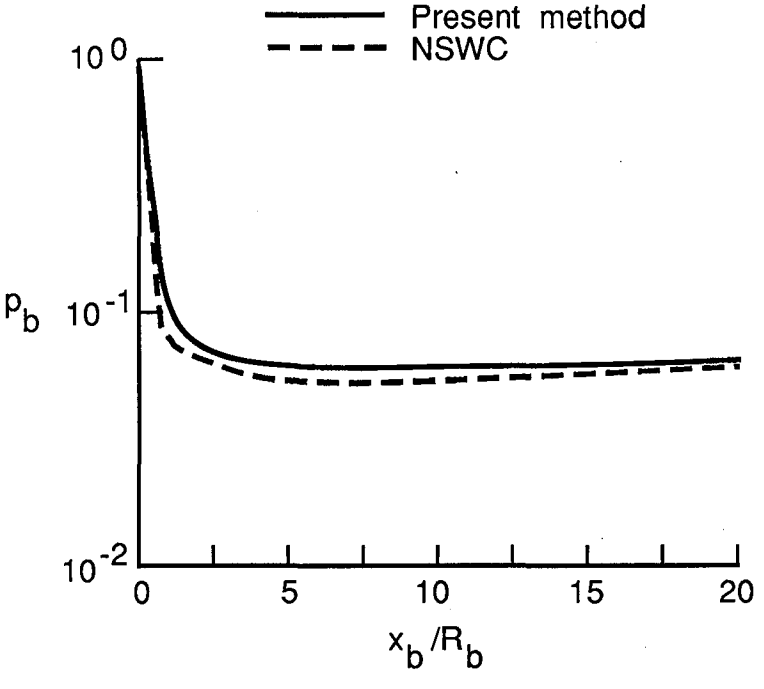

Figure 4. Axial-surface pressure distribution on blunt cone with $\theta_c = 10°$, $\alpha = 0°$, and $M_\infty = 5$.

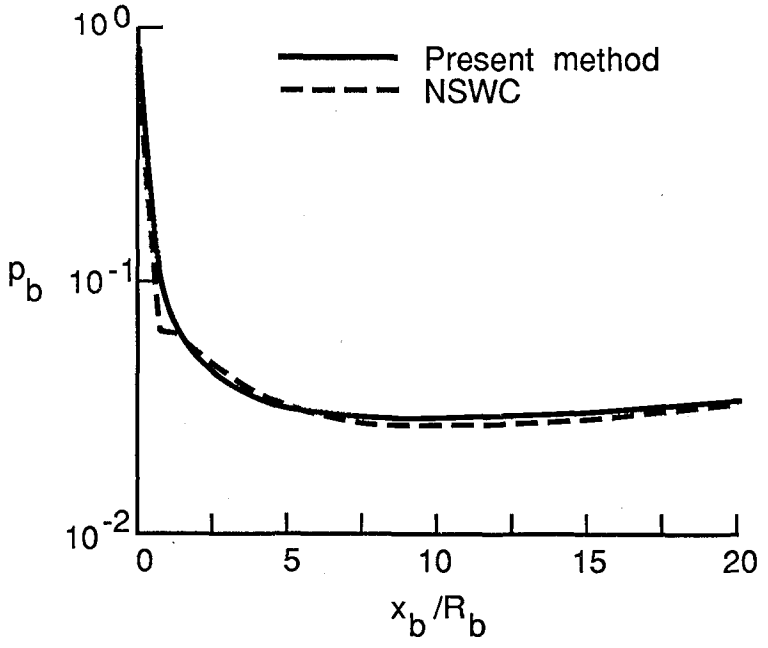

Figure 5. Axial-surface pressure distribution on blunt cone with $\theta_c = 10°$, $\alpha = 0°$, and $M_\infty = 20$.

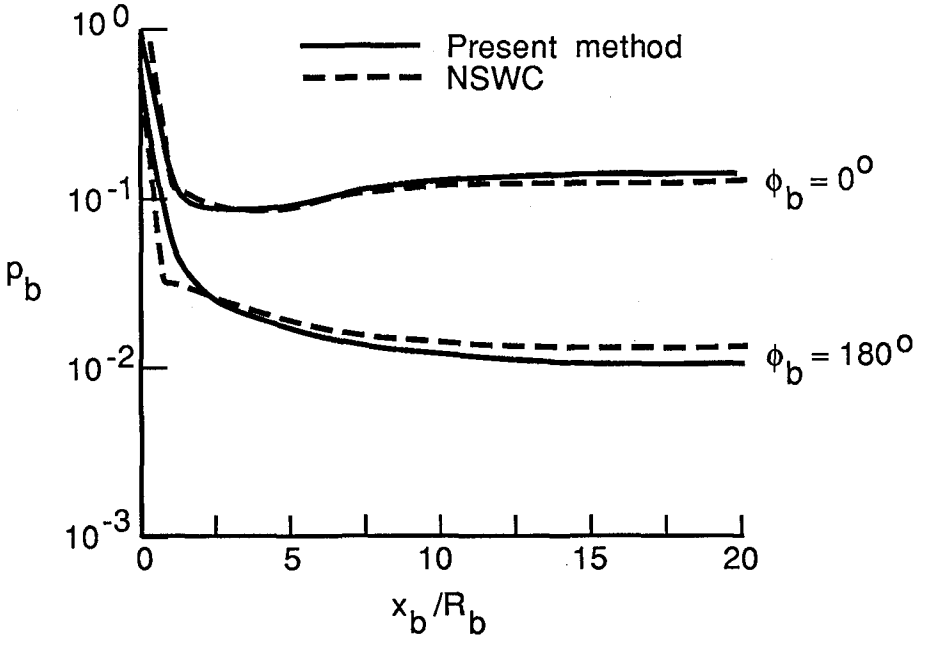

Figure 6. Axial-surface pressure distribution on blunt cone with $\theta_c = 10°$, $\alpha = 10°$, and $M_\infty = 10$.

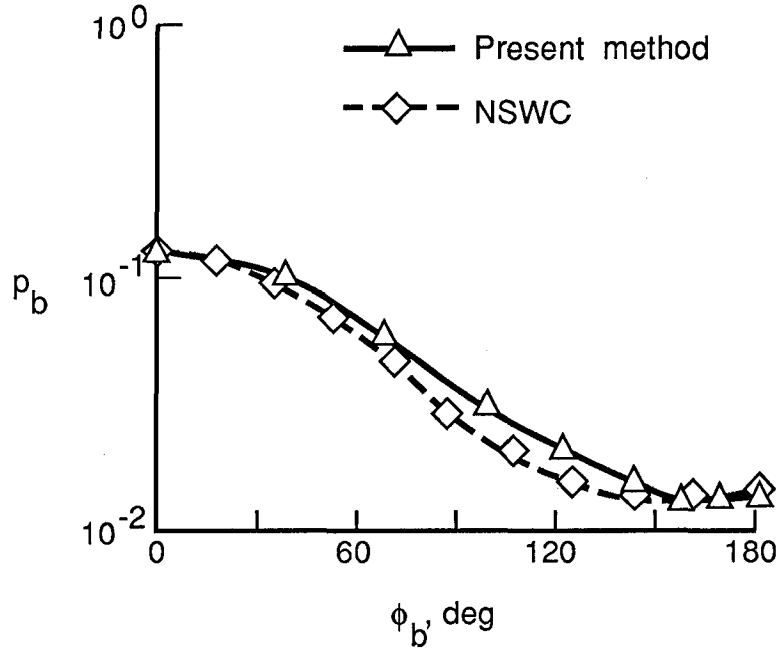

Figure 7. Circumferential surface pressure distribution on blunt cone with $\theta_c = 10°$, $\alpha = 10°$, $M_\infty = 10$, and $x_b/R_b = 9.6$.

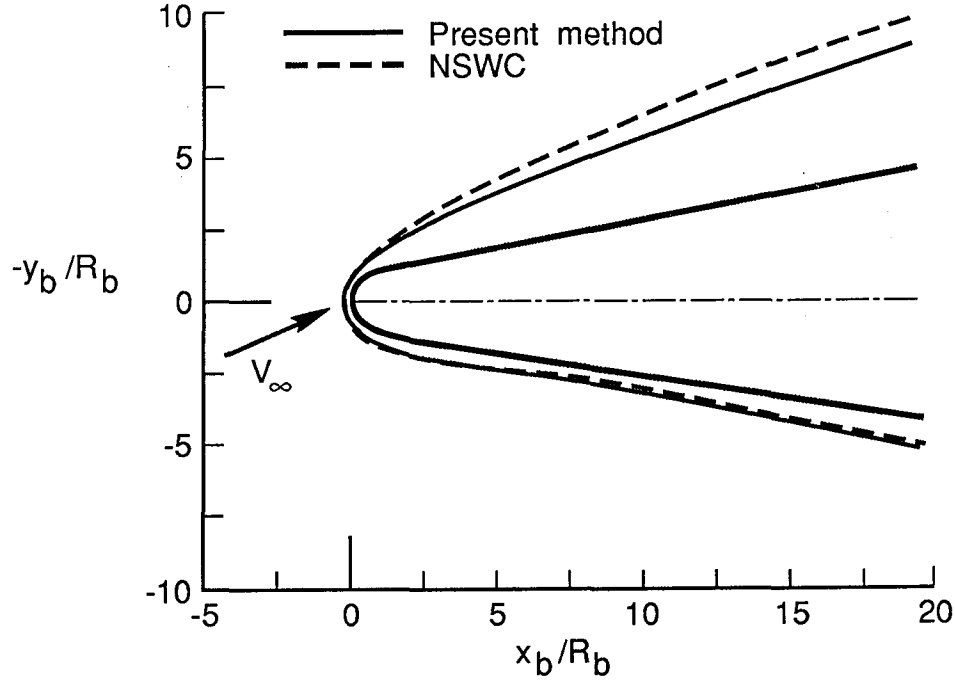

Figure 8. Shock shape in windward and leeward planes of symmetry for blunt cone with $\theta_c = 10°$, $\alpha = 10°$, and $M_\infty = 10$.

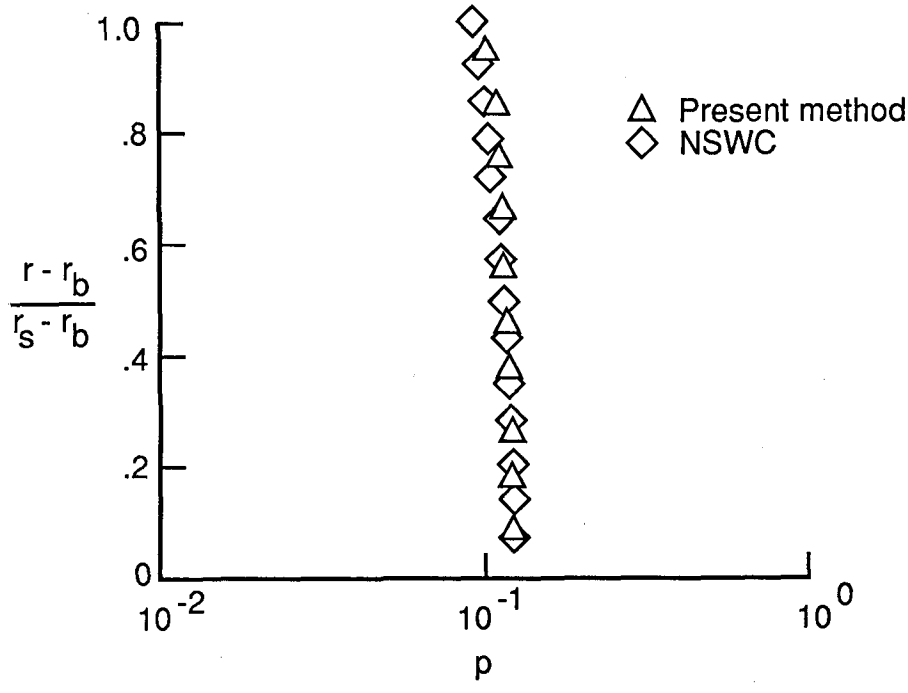

Figure 9. Radial profile of pressure with $\theta_c = 10°$, $\alpha = 10°$, $M_\infty = 10$, $x_b/R_b = 9.6$, and $\phi_b = 0°$.

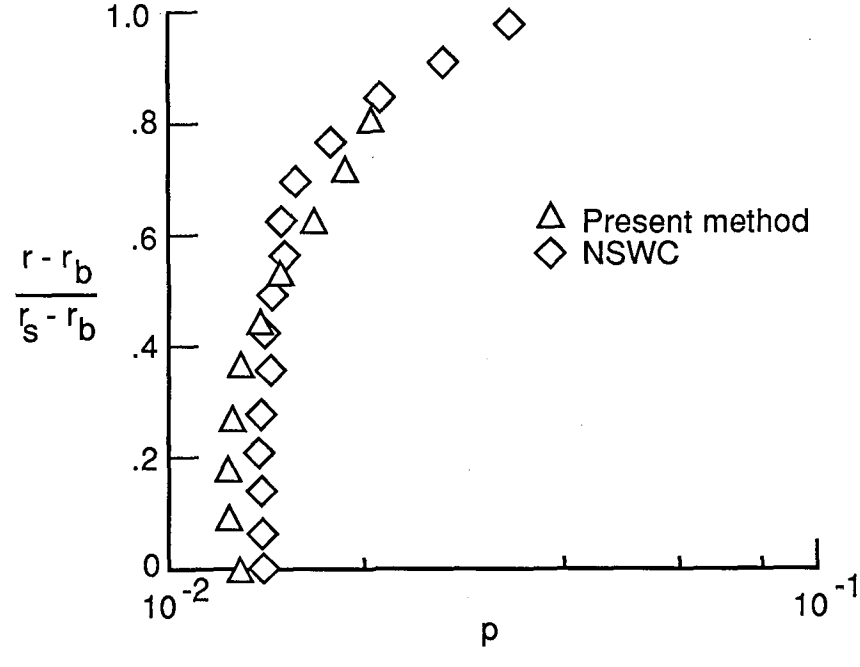

Figure 10. Radial profile of pressure with $\theta_c = 10°$, $\alpha = 10°$, $M_\infty = 10$, $x_b/R_b = 9.6$, and $\phi_b = 180°$.

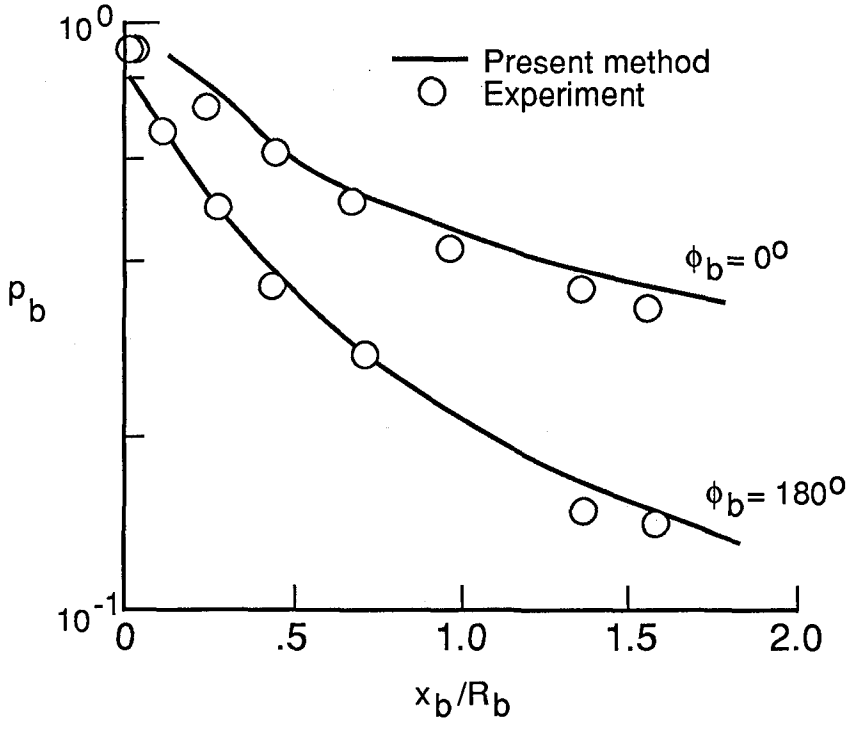

Figure 11. Axial-surface pressure distribution on paraboloid with $\alpha = 8°$ and $M_\infty = 9.9$.

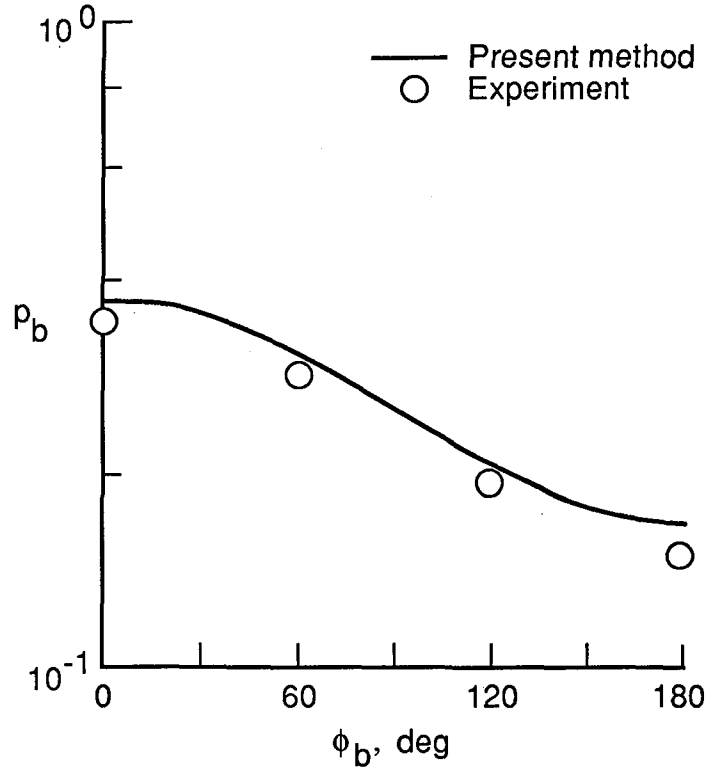

Figure 12. Circumferential surface pressure distribution on paraboloid with $\alpha = 8°$, $M_\infty = 9.9$, and $x_b/R_b = 1.38$.

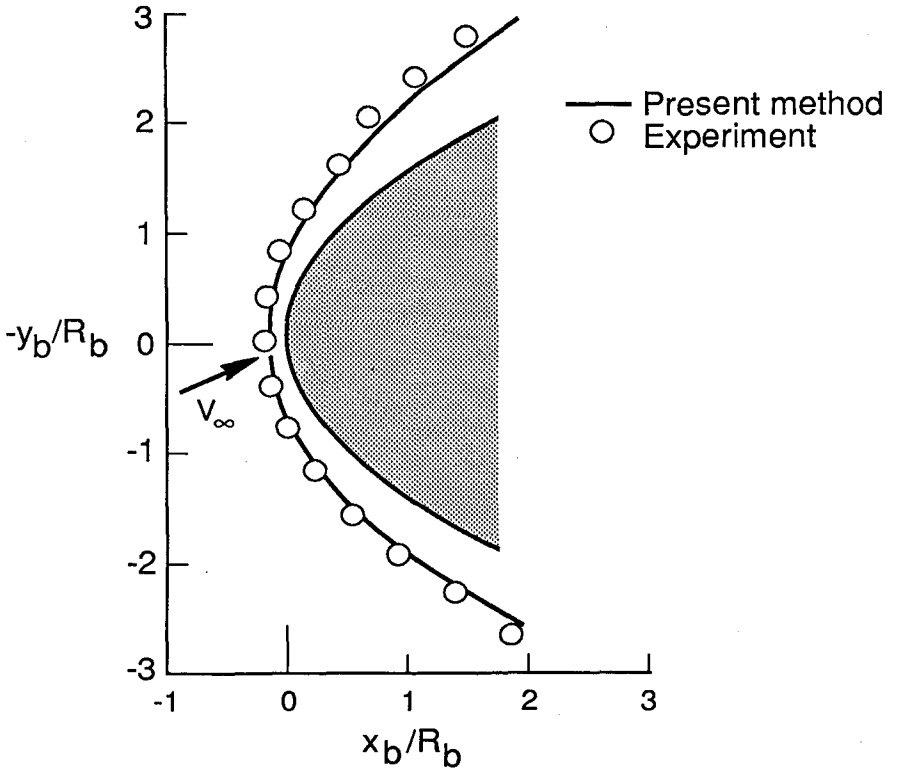

Figure 13. Shock shape in windward and leeward planes of symmetry for paraboloid with $\alpha = 8°$ and $M_\infty = 5.73$.

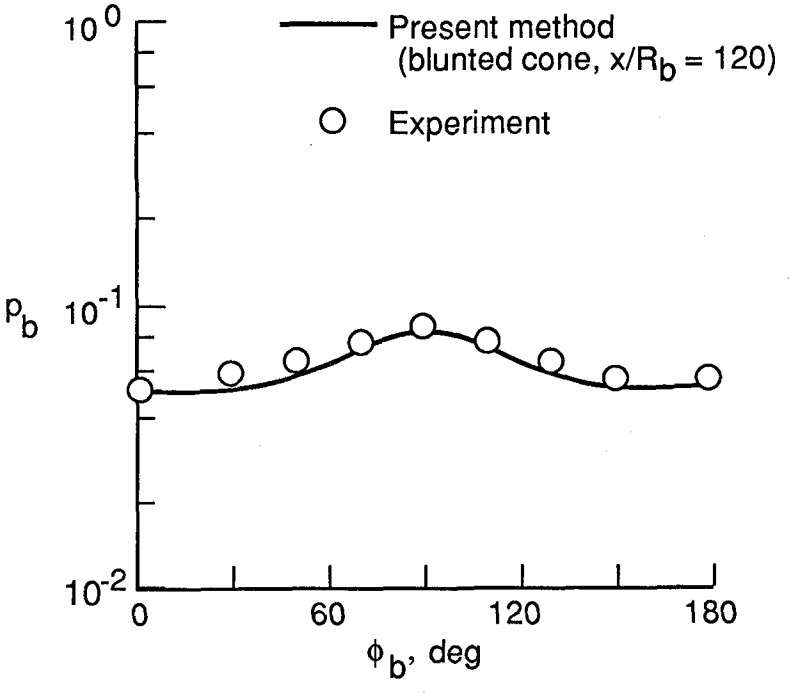

Figure 14. Circumferential surface pressure distribution on 1.5 elliptical cone with $\alpha = 0°$, $M_\infty = 10$, and $\theta_c = 10.26°$ ($\phi_b = 0°$).

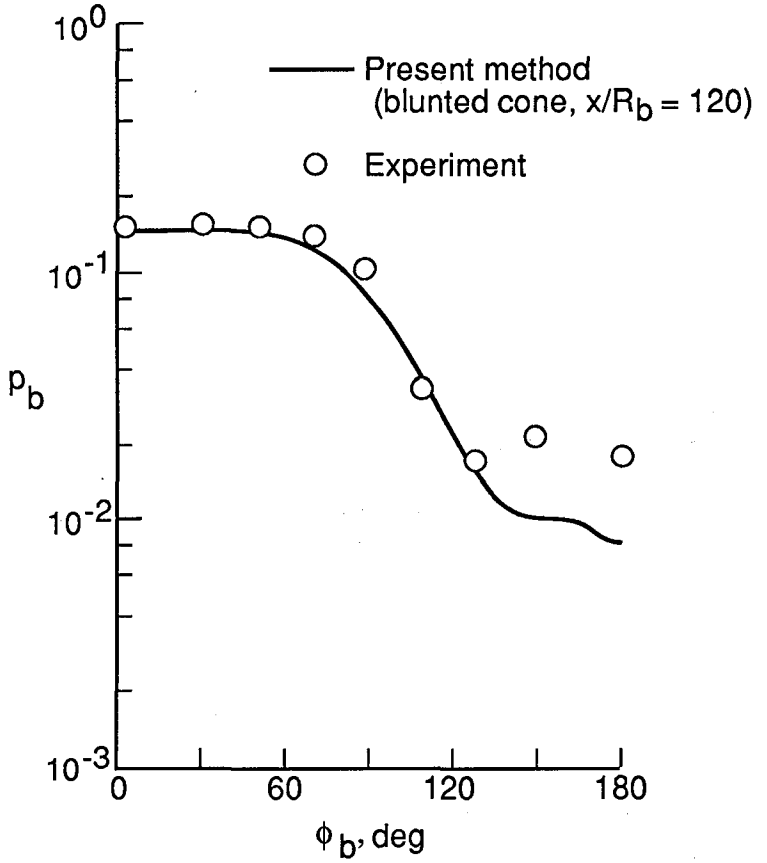

Figure 15. Circumferential surface pressure distribution on 1.5 elliptical cone with $\alpha = 10°$, $M_\infty = 10$, and $\theta_c = 10.26°$ ($\phi_b = 0°$).

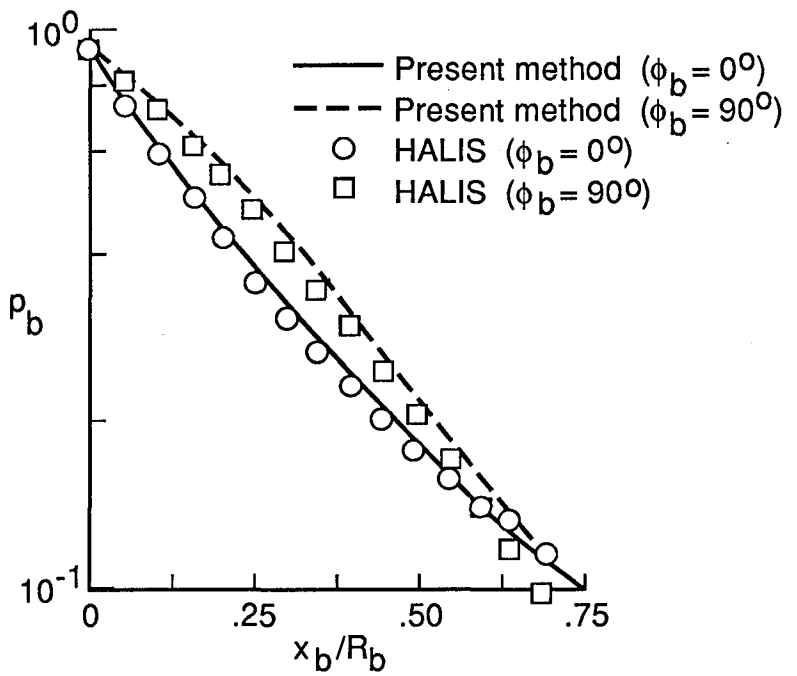

Figure 16. Axial-surface pressure distribution on 1.5 elliptical nose with $\alpha = 0°$ and $M_\infty = 10$.

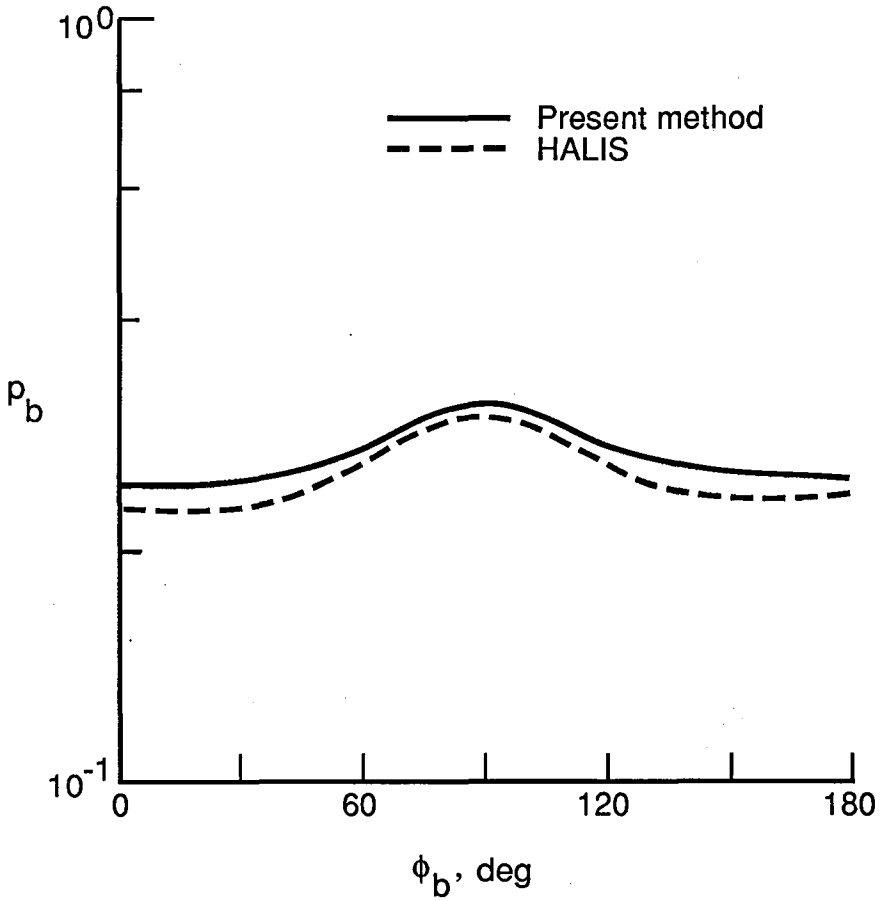

Figure 17. Circumferential surface pressure distribution on 1.5 elliptical nose with $\alpha = 0°$, $M_\infty = 10$, and $x_b/R_b = 0.4$.

NASA
National Aeronautics and Space Administration

Report Documentation Page

1. Report No.	2. Government Accession No.	3. Recipient's Catalog No.
NASA TP-3018		

4. Title and Subtitle	5. Report Date
An Approximate Method for Calculating Three-Dimensional Inviscid Hypersonic Flow Fields	August 1990
	6. Performing Organization Code
7. Author(s)	8. Performing Organization Report No.
Christopher J. Riley and Fred R. DeJarnette	L-16745
9. Performing Organization Name and Address	10. Work Unit No.
NASA Langley Research Center Hampton, VA 23665–5225	506-40-91-01
	11. Contract or Grant No.
12. Sponsoring Agency Name and Address	13. Type of Report and Period Covered
National Aeronautics and Space Administration Washington, DC 20546–0001	Technical Paper
	14. Sponsoring Agency Code

15. Supplementary Notes

Christopher J. Riley: Langley Research Center, Hampton, Virginia.
Fred R. DeJarnette: North Carolina State University, Raleigh, North Carolina.

16. Abstract

An approximate solution technique has been developed for three-dimensional, inviscid, hypersonic flows. The method uses Maslen's explicit pressure equation and the assumption of approximate stream surfaces in the shock layer. This approximation represents a simplification of Maslen's asymmetric method. The present method presents a tractable procedure for computing the inviscid flow over three-dimensional surfaces at angle of attack. The solution procedure involves iteratively changing the shock shape in the subsonic-transonic region until the correct body shape is obtained. Beyond this region, the shock surface is determined by using a marching procedure. Results are presented herein for a spherically blunted cone, a paraboloid, and an elliptical cone at angle of attack. The calculated surface pressures are compared with experimental data and finite-difference solutions of the Euler equations. Shock shapes and profiles of pressure are also examined. Comparisons of the results of the present method with experimental data and detailed predictions are very good. Since the present method provides a very rapid computational procedure, it can be used for parametric or preliminary design applications. A useful application would be to incorporate a heating procedure for aerothermal studies.

17. Key Words (Suggested by Authors(s))	18. Distribution Statement
Inviscid flow Hypersonic flow Three-dimensional flow Approximate methods	Unclassified—Unlimited Subject Category 34

19. Security Classif. (of this report)	20. Security Classif. (of this page)	21. No. of Pages	22. Price
Unclassified	Unclassified	23	A03

For sale by the National Technical Information Service, Springfield, Virginia 22161-2171

National Aeronautics and
Space Administration
Code NTT-4

Washington, D.C.
20546-0001

BULK RATE
POSTAGE & FEES PAID
NASA
Permit No. G-27